Journal of Power Sources 243 (2013) 260–266

Contents lists available at SciVerse ScienceDirect

Journal of Power Sources

journal homepage: www.elsevier.com/locate/jpowsour

Influence of thermal history on the electrochemical properties of Li[$Ni_{0.5}Mn_{1.5}$]O_4

Guoqiang Liu [a,b], Kyu-Sung Park [b], Jie Song [b], John B. Goodenough [b,*]

[a] School of Material and Metallurgy, Northeastern University, Shenyang 110819, China
[b] Materials Science and Engineering Program and Texas Materials Institute, The University of Texas at Austin, Austin, TX 78712, United States

HIGHLIGHTS

- $LiNi_{0.5}Mn_{1.5}O_4$ was synthesized at 900 °C and cooled in different ways.
- $LiNi_{0.5}Mn_{1.5}O_4$ synthesized at a slow cooling rate exhibited good cycle performance at 55 °C.
- The reason of capacity decay at elevated temperature was deduced from experiment.

ARTICLE INFO

Article history:
Received 6 May 2013
Received in revised form
29 May 2013
Accepted 31 May 2013
Available online 10 June 2013

Keywords:
Li-ion battery
Cathode
High-voltage
Surface chemistry

ABSTRACT

The oxygen-stoichiometric spinel Li[$Ni_{0.5}Mn_{1.5}$]O_4 is an insulator with ordered Ni(II) and Mn(IV). Although it delivers 4.7 V versus Li, the ordered phase gives poor performance as the cathode of a Li-ion battery. Here we demonstrate control of the degree of cation order by adjusting the oxygen stoichiometry with thermal history of the synthesis rather than by doping 2M(III) for Ni(II) + Mn(IV) (M = Cr, Mn, Fe, Co, Al, Ga). We report retention of capacity near 100 mAh g^{-1} at room temperature at 10C/10C charge/discharge rate with little capacity fade; at 55 °C, a capacity fade occurs as a result of reaction with the electrolyte, but it is reduced to a level comparable to that obtained by doping.

1. Introduction

The spinel Li[$Ni_{0.5}Mn_{1.5}$]O_4 is considered a promising cathode material for a Li-ion battery owing to its high working voltage of *ca.* 4.7 V versus Li even though this voltage is well-above the HOMO voltage (*ca.* 4.1 V versus Li) of the organic liquid-carbonate electrolyte normally used. The electrochemical properties of nominal Li[$Ni_{0.5}Mn_{1.5}$]O_4 as a cathode material depend not only on the size and morphology of the spinel particles, but also on the stability of their surface chemistry in the charged state *vis-à-vis* the organic liquid-carbonate electrolyte [1–8].

Oxygen stoichiometric Li[$Ni_{0.5}Mn_{1.5}$]O_4 is an electronic insulator containing Ni(II) and Mn(IV) ions ordered on the spinel octahedral sites at room temperature; oxidation of Ni(II) at 4.7 V versus Li creates a reaction between the surface Ni atoms and the electrolyte that produces a severe capacity fade on cycling. Disordering the Ni(II) and Mn(IV), which is accompanied by the introduction of Mn(III) by loss of oxygen, has been shown to sharply reduce the capacity fade. Previous workers [9–12] have substituted M(III) ions Cr, Mn, Fe, Co, Al, Ga into the octahedral sites in order to disorder the $Ni(II)_{0.5}Mn(IV)_{1.5}$ array. These studies have reduced the capacity fade, and it has been suggested that this reduction is achieved by displacing oxidized Ni from the surface. Here we report an investigation of the role of thermal history in the synthesis of Li[$Ni_{0.5}Mn_{1.5}$]O_4 and demonstrate that control of the oxygen stoichiometry can control both the degree of Ni(II), Mn(IV) ordering and the amount of oxidized Ni on the surface to improve stabilization of the surface chemistry equal to the stabilization achieved by M(III) substitution.

Previous studies [8,13] have clarified the following: (1) Li[$Ni_{0.5}Mn_{1.5}$]O_4 loses oxygen reversibly on heating/cooling in air in the interval $700 \leq T \leq 900$ °C via a reversible structural change; the oxygen-deficient spinel obtained on heating above 700 °C

* Corresponding author. Tel.: +1 512 471 1646; fax: +1 512 471 7681.
E-mail address: jgoodenough@mail.utexas.edu (J.B. Goodenough).

0378-7753/$ – see front matter © 2013 Published by Elsevier B.V.
http://dx.doi.org/10.1016/j.jpowsour.2013.05.189

segregates into a nickel-rich rock-salt phase and a Mn-rich spinel phase containing Mn(III), but this structural change is reversible on slow-cooling in air. (2) The cooling rate from 900 °C through 700 °C in air determines the oxygen stoichiometry at room temperature and its distribution between the surface and the bulk core, thereby controlling the degree of Ni(II), Mn(IV) ordering of the spinel phase and the distribution of the rock-salt phase. (3) Some Ni-rich rock-salt phase remains in the product if the cooling rate though 700 °C is too fast, and the size and distribution of the rock-salt nano-clusters can be expected to change with the cooling rate. Electrochemical characterization has shown the best results are achieved where slow-cooled cathode particles are single-phase spinel to powder X-ray diffraction, but still retain some Mn(III) and little long-range order of Ni(II) and Mn(IV). These observations motivated us to investigate whether precise control of the thermal history of synthesis may provide cathode particles containing a stabilized surface chemistry in which strongly oxidized surface Ni is minimized.

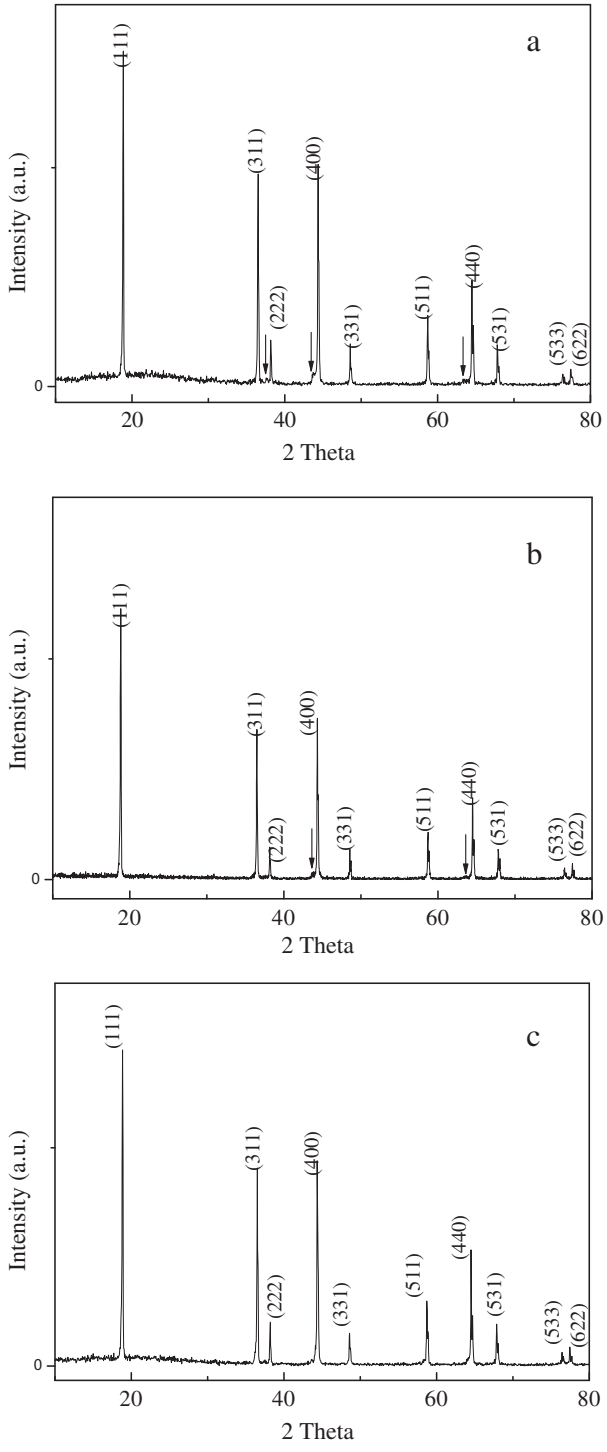

Fig. 1. XRD patterns of the as prepared sample 1 (a), 2 (b) and 3 (c), the arrows represent the rock-salt phase.

2. Experimental

Stoichiometric amounts of $LiNO_3$, $Ni(NO_3)_2 \cdot 6H_2O$ and $Mn(CH_3COO)_2 \cdot 4H_2O$ were dissolved in distilled water and stirred to obtain a clear aqueous solution. To compensate for the lithium loss at high temperature, a small amount of extra Li salt was added to this solution. In parallel, glycolic acid aqueous solution was also prepared with a 2:1 molar ratio of total metal ions to glycolic acid. The two solutions were mixed and stirred; the water was then thermally evaporated at 120 °C to make a gel. The dried gel was calcined at 900 °C for 12 h in air. Finally, different products were obtained by cooling down from 900 °C to room temperature at different cooling rates. The cooling rates were 3 °C min^{-1} for sample 1 and 1.2 °C min^{1} for sample 2. Sample 3 was first cooled to 650 °C at a 3 °C min^{-1} rate and annealed for 20 h before cooling to room temperature at 3 °C min^{-1}.

X-ray diffraction patterns were obtained with a Philips X-ray diffractometer equipped with Cu Kα radiation. The powder morphologies of the products were examined with a Hitachi scanning electron microscope (SEM), and a FEI-TECNAI G2F20/America transmission electron microscope. Raman spectra were obtained with a Renishaw in Via Raman Microscope with a 442-nm blue laser beam.

Electrochemical properties were measured with coin half-cells composed of $Li[Ni_{0.5}Mn_{1.5}]O_4$ as cathodes, a metallic-lithium anode, 1 mol L^{-1} $LiPF_6$ in 1:1 volume mixture of diethyl carbonate/ethylene carbonate as electrolyte, and a Celgard polypropylene separator. The cathodes were prepared by mixing 85 wt% active material with 10 wt% acetylene black and 5 wt% PVDF binder in N-Methyl-2-Pyrrolidone (NMP); the slurry was cast on aluminum foil, dried in an oven, and punched into circular discs of 0.95 cm in diameter. The cathode loading was 6 mg cm^{-2}. All coin cells were assembled in an argon-filled glove box. The cells were galvanostatically cycled under different current densities between 3.50 V and 4.90 V at room temperature and 55 °C, and also between 4.50 and 4.90 V at 55 °C.

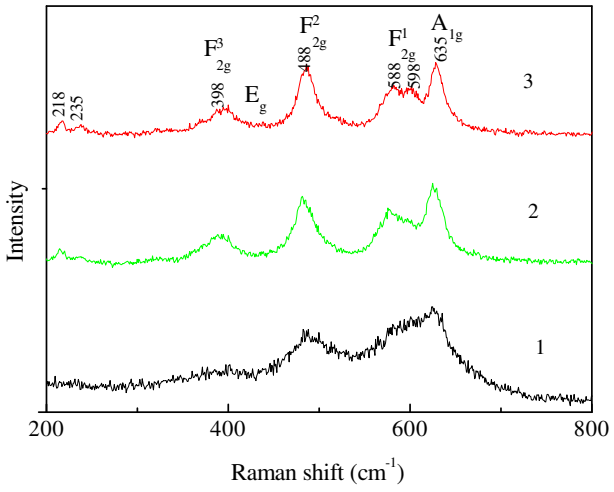

Fig. 2. Raman spectra of the as prepared sample 1, 2 and 3.

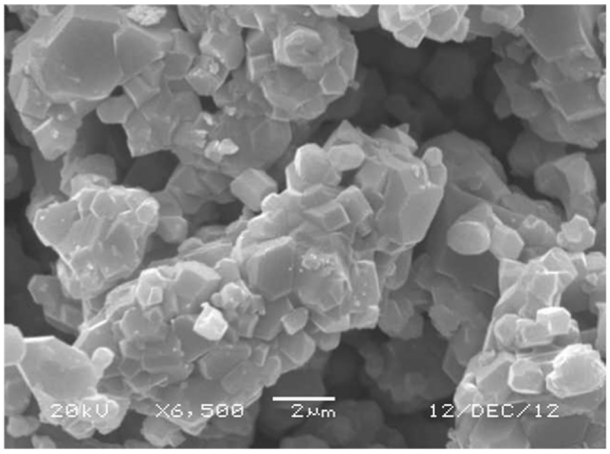

(a)

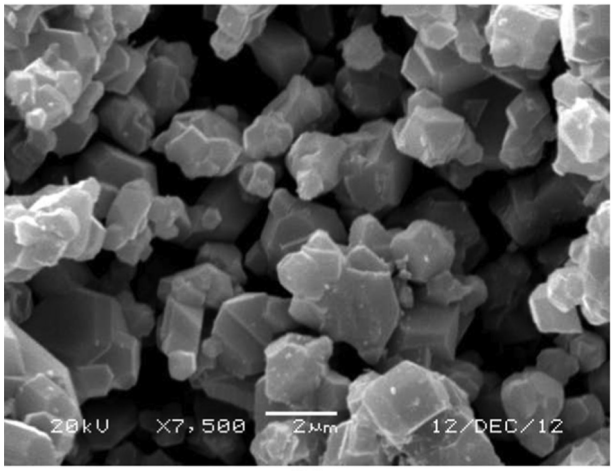

(b)

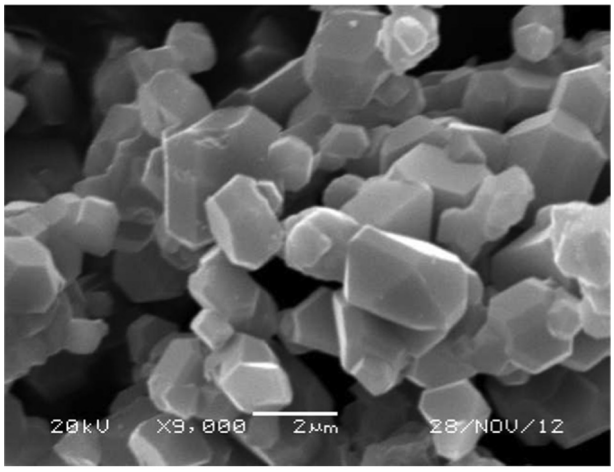

(c)

Fig. 3. Scanning electron micrographs of the as prepared sample 1 (a), 2 (b) and 3 (c).

3. Results and discussion

The spinel $Li[Ni_{0.5}Mn_{1.5}]O_4$ with disordered Ni/Mn on the octahedral sites has the face-centered-cubic *Fd*3*m* structure; long-range ordering of the Ni/Mn gives a primitive simple-cubic $P4_332$ structure [14]. The $P4_332$ structure gives additional peaks at 24.34°, 26.70°, 32.80°, and 34.70°. Fig. 1 shows the powder XRD patterns for the three prepared samples. None of these additional peaks are present in any of the three patterns, which shows there is no (visible to powder X-ray diffraction) long-range ordering of Ni^{2+} and Mn^{4+} in any of the samples. However, the pattern for sample 1 shows weak rock-salt impurity peaks at 37.5°, 43.7°, and 63.6°. The amount of the rock-salt impurity phase is smaller in sample 2 and is absent to powder X-ray diffraction in sample 3. The cubic lattice parameters, calculated by the generalized least-squares method, are 8.1811 Å, 8.1734 Å, and 8.1603 Å for samples 1, 2, and 3, respectively. The larger the lattice parameter, the larger the concentration of Mn(III) ions.

The degree of Ni/Mn ordering in the surface layers of the three samples was investigated with Raman Spectroscopy. The octahedral $Mn(Ni)O_6$ structures have *Oh* symmetry where vibrations A_{1g}, E_g, and F_{2g} are Raman active [15–17]. Fig. 2 shows the Raman spectra of the as-prepared $LiNi_{0.5}Mn_{1.5}O_4$ samples. In sample 3, Raman-active bands are at 635 cm^{-1}, 588 cm^{-1}, 600 cm^{-1}, 488 cm^{-1}, 398 cm^{-1}, 218 and 235 cm^{-1}. The peaks at 635 cm^{-1} can be assigned to the A_{1g} mode, reflecting symmetric M–O stretching vibration of MO_6 groups. The peaks at 588 cm^{-1} and 600 cm^{-1} indicate Ni^{2+}/Mn^{4+} cation ordering [18]. Therefore, sample 3 shows regions of short-range order. Sample 2 lacks Raman active bands at 235 cm^{-1} and 600 cm^{-1}, so there is less short-range order. In sample 1, Raman active bands are only at 635 cm^{-1} and 488 cm^{-1}; therefore this sample is disordered.

Fig. 3 shows the morphological features of the samples as obtained by scanning electron microscopy. The powder samples are polyhedral-shaped and well-crystallized. Most particles range from 1 to 3 μm in size. The morphology of the as prepared product mainly depends on the synthesizing temperature and time. Because the three samples were synthesized at the same temperature and time, their morphologies should almost have the same size and shape. Minor morphology differences among the three samples exist owing to different cooling rates. For sample 1, there is serious particle aggregation. The samples 2 and 3 have less and least particle aggregation, respectively.

Fig. 4 shows the electron diffraction patterns of sample 3 in the [110] zone. It can be found that some unexpected reflections are found in the electron diffraction pattern, which should be forbidden by the F*d*3*m* space group. The occurrence of the superlattice pattern is attributed to the Ni^{2+}/Mn^{4+} ordering,

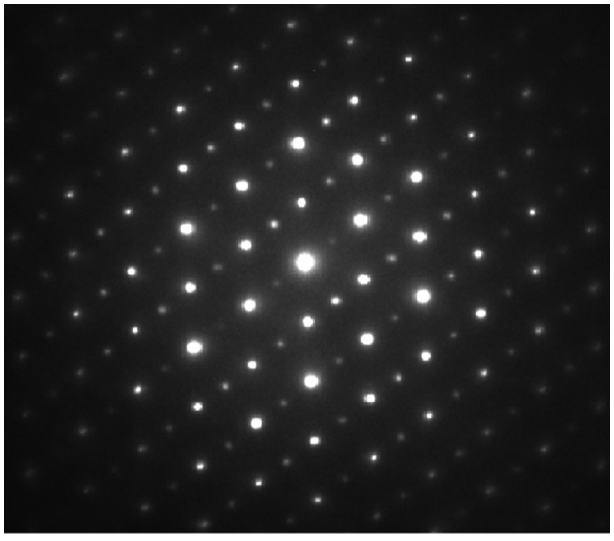

Fig. 4. Electron diffraction patterns of sample 3 in the [110] zone.

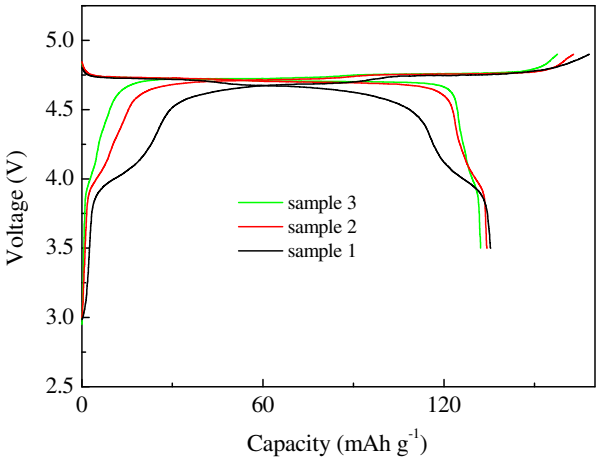

Fig. 5. Charge and discharge curves of the as prepared samples at the low current density of 0.1C/0.1C rate at room temperature.

indicating the coexistence of the ordered phase ($P4_332$) in the sample [4].

In order to analyze the charge/discharge behaviors of the samples, a C/10-rate cycling test was conducted; Fig. 5 and Table 1 show the results. The two distinct plateaus at around 4.7 V are attributed to the Ni(III)/Ni(II) and Ni(IV)/Ni(III) redox couples. The 4-V shoulder originates from the oxidation and reduction of the Mn(IV)/Mn(III) couple. Sample 1 has a disordered Ni/Mn configuration and the greatest concentration of Mn(III). Its 4.7 V plateau is short because some Ni separated from $Li[Ni_{0.5}Mn_{1.5}]O_4$ to form a Ni-rich rock-salt phase. Sample 3 has regions of longer-range Ni/Mn ordering and the smallest amount of Mn(III). Although its 4.7 V plateau is the longest, its total capacity is the smallest among the samples during both charge and discharge. The data show that to increase the capacity at 4.7 V, the rock-salt impurity phase should be reduced. The data for sample 2 are between those of the other two samples. The presence of Mn(III) and short-range Ni/Mn ordering improves the electrochemical properties as indicated in previous studies.

In order to evaluate the rate capability of the samples, 1C-charge/1C-discharge, 5C-charge/5C-discharge, and 10C-charge/10C-discharge rates were also investigated. Fig. 6(a) shows the first charge/discharge voltage curves at the 1C/1C charge/discharge condition. Samples 1, 2, and 3 delivered discharge specific capacities of 132.5, 131 and 126.1 mAh g^{-1}, respectively. The trend in the capacity is the same as with the low-current charge/discharge rate. Fig. 6(b) shows the cycle performance of the samples. After 100 cycles, the capacity retentions were 94.5%, 96.4% and 87.9% for samples 1, 2 and 3, respectively. The Ni/Mn ordering and the amount of Mn(III) significantly affect the rate of capacity fade.

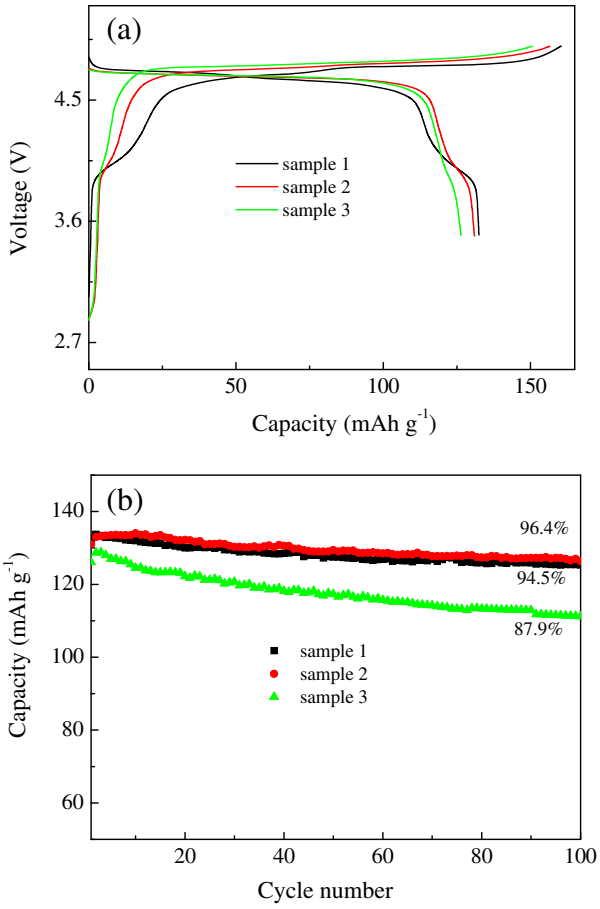

Fig. 6. Electrochemical properties of the as prepared samples at 1C/1C rate. (a) First charge–discharge curves; (b) cycle performance.

Fig. 7(a) and (b) show the charge and discharge voltage curves of the samples at the 5C/5C and 10C/10C rates after an initial activation cycle at 1C/1C rate. At the 5C/5C rate, the discharge capacities were 102.1 mAh g^{-1}, 105.3 mAh g^{-1} and 91.3 mAh g^{-1} for samples 1, 2 and 3, respectively. At the 10C/10C rate, the capacities were 87.8 mAh g^{-1}, 97.1 mAh g^{-1} and 68.6 mAh g^{-1} for samples 1, 2 and 3, respectively. From the charge and discharge voltage curves at the 10C/10C rate, notable differences between the samples in the charge and discharge plateaus can be observed. Sample 2 has the smallest over-voltage while sample 3 has the largest, which means that sample 2 has the best rate capability. Fig. 7(c) shows the room-temperature cycle performance of the samples at the 5C/5C and 10C/10C rates. All the samples show good cycle performance at room temperature.

The electrochemical property of an electrode material at elevated temperatures is an important consideration because

Table 1
Structural characteristics and discharge behaviors of the as prepared samples at slow current rate 0.1/0.1 C.

Sample	Discharge capacity (mAh g^{-1})		Amount of Mn^{3+} per formula unit of $Li[Ni_{0.5-x}Mn_{1.5+x}]O_4$[c]	Ordering	Lattice parameters (Å)
	4.7 V region[a]	4 V region[b]			
(1) Fast-cooled $Li[Ni_{0.5}Mn_{1.5}]O_4$	113.4	22	0.149	Disordered	8.1811
(2) Slow-cooled $Li[Ni_{0.5}Mn_{1.5}]O_4$	123.7	10.5	0.071	Short-range ordered	8.1734
(3) Annealed $Li[Ni_{0.5}Mn_{1.5}]O_4$	125.1	7	0.047	Long-range ordered	8.1603

[a] The 4.7 V region is the voltage range of 4.90–4.40 V.
[b] The 4 V region is the voltage range of 4.40–3.50 V.
[c] The amount of Mn^{3+} was calculated by the theoretical capacity of $Li[Ni_{0.5}Mn_{1.5}]O_4$ which is about 147 mAh g^{-1}.

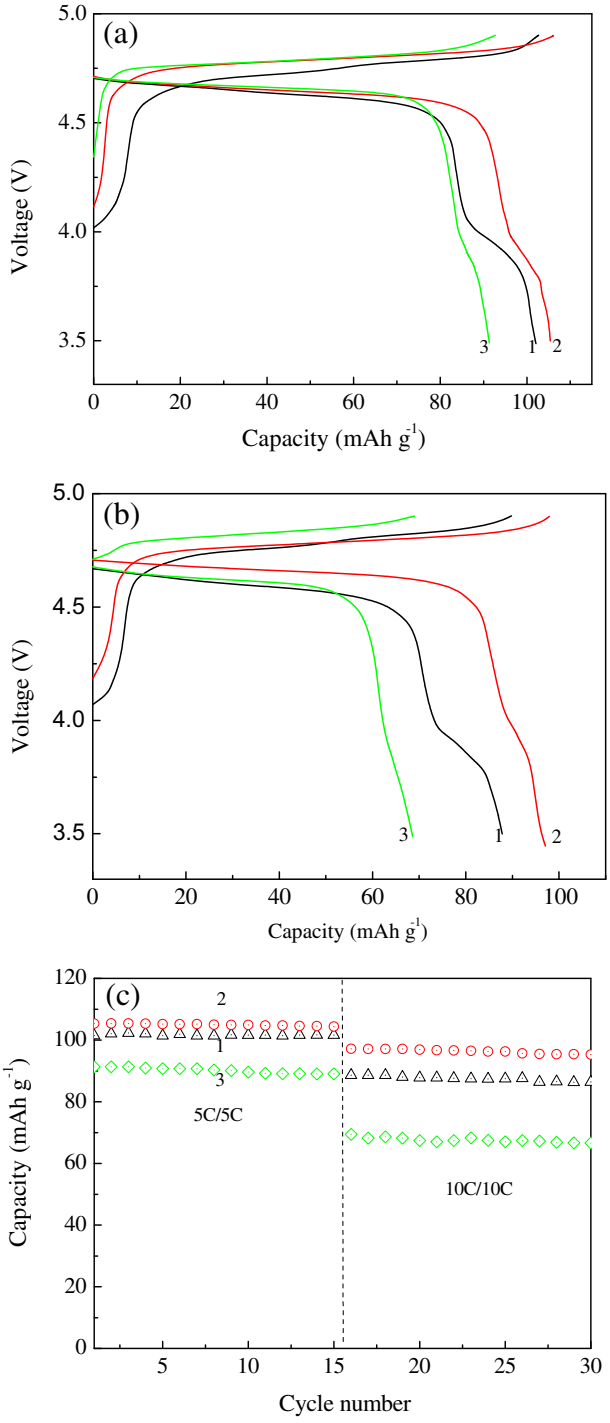

Fig. 7. Rate capabilities of the as prepared samples at 5C/5C and 10/10 C rates at room temperature. (a) Charge–discharge curves at 5C/5C; (b) charge–discharge curves at 10C/10C; (c) cycle performances.

electrode materials undergo faster capacity fading at higher temperatures. The charge and discharge behaviors at 55 °C were investigated for these samples. Fig. 8(a) shows the first 1C/1C charge and discharge voltage curves of the as-prepared samples. The discharge capacities are 133.5 mAh g^{-1}, 131.8 mAh g^{-1} and 126.5 mAh g^{-1} for samples 1, 2 and 3, respectively. The discharge capacities at elevated temperature are slightly higher than those at room temperature. Fig. 8(b) shows the cycle performances with the 1C/1C charge/discharge condition at 55 °C. After 100 cycles, the

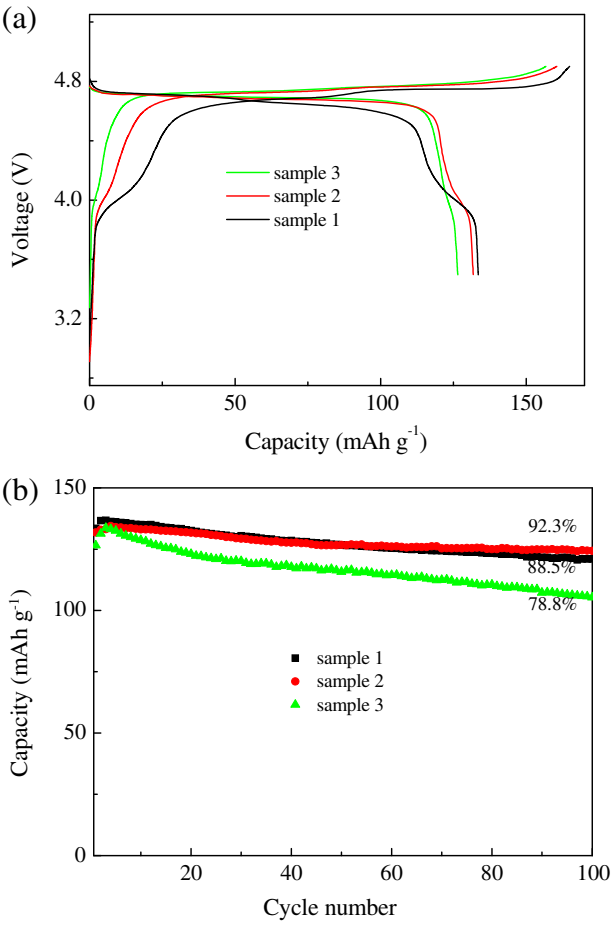

Fig. 8. Electrochemical properties of the as prepared samples at 1C/1C rate. (a) First charge–discharge curves; (b) Cycle performance.

capacity retention is 88.5%, 92.3% and 78.8% for sample 1, 2, and 3, respectively. The capacity decays faster at elevated temperature than at room temperature, especially in the sample with regions of longer-range order.

The charge/discharge voltage curves of sample 2 at room temperature and 55 °C are compared in Fig. 9; the cell impedance is lower at elevated temperature than at room temperature.

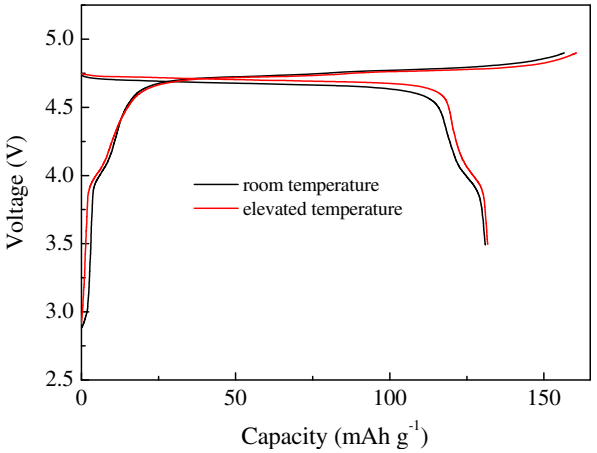

Fig. 9. Comparison of charge–discharge curves of sample 2 between room temperature and elevated temperature.

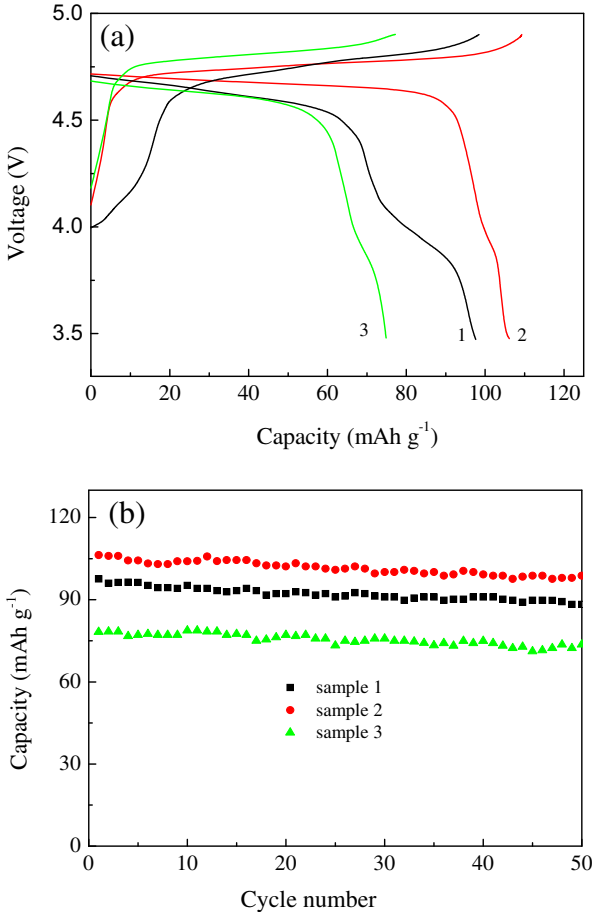

Fig. 10. Rate capabilities of the as prepared samples at 10C/10C rates and at elevated temperature of 55 °C. (a) Charge–discharge curves at 10C/10C; (b) cycle performances at 10C/10C.

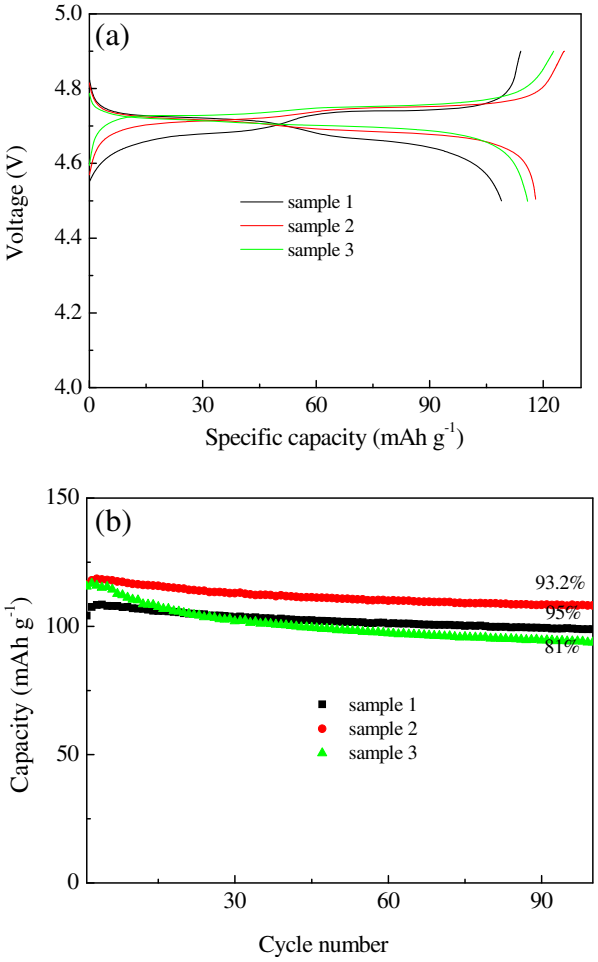

Fig. 11. Electrochemical properties at 55 °C of the as prepared samples at 1C/1C rate from 3.5 V to 4.9 V. (a) Charge–discharge curves at 10C/10C; (b) cycle performances at 10C/10C.

The high-rate cyclability at 10C/10C and at 55 °C was also measured, as shown in Fig. 10(a) and (b). These results show that the samples can support high current rates at elevated temperature. A comprehensive comparison of the electrochemical properties is summarized in Table 2.

In order to distinguish the capacity fade resulting from oxidation of the electrolyte by oxidized surface Ni and from dissolution of Mn(II) as a result of disproportionation of surface Mn(III), we cycled coin cells at 55 °C at 1C/1C between 4.5 and 4.9 V where reduction of Mn(IV) to Mn(III) does not occur. Fig. 11 shows the test results. Sample 1 has the largest concentration of the rock-salt phase, which does not cycle; it also has the largest concentration of disordered, Mn-rich spinel phase, which gives a large capacity in Fig. 11(b). Sample 3 has the least concentration of the rock-salt phase and the highest concentration of the ordered spinel; it has a poorer rate capability and therefore a lower capacity at 1 C rate. The slow-cooled sample 2, with an intermediate rock-salt concentration and only a little short-range ordering of the spinel phase, exhibits the highest capacity at 1 C and 55 °C. All three samples exhibited a better cycling performance, as shown in Fig. 11(b), when cycled between 3.5 and 4.9 V versus Li. The fast-cooled sample 1 showed the greatest improvement with 95% capacity retention after 100 cycles, sample 3 the lowest, and sample 2 an intermediate improvement. Clearly trapping of Ni in a Ni-rich rock-salt phase near the surface reduces the oxidized surface Ni responsible for an oxidation of the electrolyte that contributes to the capacity fade on cycling. This effect is not completely eliminated in the slow-cooled Sample 2 since there is some Mn^{3+}-rich spinel phase at the surface containing oxidizable Ni.

Table 2
Rate capabilities of the as prepared samples at room temperature and at elevated temperature 55 °C.

Sample	Discharge capacity (mAh g^{-1})					
	0.1/0.1 C (RT)	1/1 C (RT)	5/5 C (RT)	10/10 C (RT)	1/1 C (55 °C)	10/10 C (55 °C)
(1) Fast-cooled $Li[Ni_{0.5}Mn_{1.5}]O_4$	135.4	132.5	102	87.8	133.5	97.6
(2) Slow-cooled $Li[Ni_{0.5}Mn_{1.5}]O_4$	134.2	131	106	97.1	131.8	106.1
(3) Annealed $Li[Ni_{0.5}Mn_{1.5}]O_4$	132.1	126.1	92.7	68.6	126.5	75

4. Conclusions

Nominal $Li[Ni_{0.5}Mn_{1.5}]O_4$ offers a high-voltage cathode (4.7 V versus Li) for the Li-ion battery, but the oxygen-stoichiometric spinel exhibits a rapid capacity fade on cycling. The electrochemical properties of nominal $Li[Ni_{0.5}Mn_{1.5}]O_4$ synthesized at 900 °C can be greatly improved by controlling the thermal history on cooling. At 900 °C, oxygen loss creates a segregation into a Ni-rich rock-salt phase and a Mn-rich spinel phase. Slow cooling through 700 °C allows a reconstitution of the spinel phase at the expense of the rock-salt phase; but by controlling the cooling rate in air, it is possible to regulate the volume fractions of the two phases since the reversible segregation reaction is not rapid. The rock-salt phase is not oxidized by extracting Li from the spinel phase, and excess Mn in the spinel phase prevents long-range order of the Ni(II) and Mn(IV) in the spinel phase that occurs in the oxygen-stoichiometric spinel. Trapping the Ni in nano-sized rock-salt clusters in a surface layer would prevent oxidation of the electrolyte by surface Ni(IV)/Ni(III) on charge; but on discharge, a Mn(III)-rich surface can result in the surface disproportionation reaction $2Mn(III) = Mn(II) + Mn(IV)$ followed by dissolution of Mn(II) into the electrolyte. Dissolution of the Mn(II) is a slower process than oxidation of the electrolyte by Ni(IV)/Ni(III) at 4.7 V versus Li. The enhanced capacity fade at 55 °C of the fast-cooled sample cycled from 3.5 to 4.9 V is, we believe, the result of an enhanced rate of Mn(II) dissolution. Too great a concentration of the rock-salt phase increases the Mn(III) concentration in the spinel phase and therefore the extent of surface disproportionation of the Mn valence; it also can be expected to increase the Li^+ electrolyte/electrode transfer impedance. Optimization of the surface rock-salt volume fraction while suppressing Ni(II), Mn(IV) long-range order in the spinel phase provides as high a reduction of capacity fade at 55 °C as has been achieved by doping with Mn(III) ions.

Acknowledgments

This work was supported by the Department of Energy Office of Basic Energy Science grant number DE-SC0005397 and the Robert A Welch Foundation, Houston, Texas Grant Number F-1066. The authors would like to thank Dr. Huifeng Li for collecting the Raman data.

References

[1] Z.X. Chen, S. Qiu, Y.L. Cao, X.P. Ai, K. Xie, X.B. Hong, H.X. Yang, J. Mater. Chem. 22 (2012) 17768–17772.
[2] G.Q. Liu, L. Wen, Y.M. Liu, J. Solid State Electrochem. 14 (2010) 2191–2202.
[3] Y.C. Jin, C.Y. Lin, J.G. Duh, Electrochim. Acta 69 (2012) 45–50.
[4] J. Xiao, X.L. Chen, P.V. Sushko, M.L. Sushko, L. Kovarik, J.J. Feng, Z.Q. Deng, J.M. Zheng, G.L. Graff, Z.M. Nie, D. Choi, J. Liu, J.G. Zhang, M.S. Whittingham, Adv. Mater. 24 (2012) 2109–2116.
[5] D.W. Shin, A. Manthiram, Electrochem. Commun. 13 (2011) 1213–1216.
[6] N.M. Hagh, F. Cosandey, S. Rangan, R. Bartynski, G.G. Amatucci, J. Electrochem. Soc. 157 (2010) A305–A319.
[7] G.B. Zhong, Y.Y. Wang, Y.Q. Yu, C.H. Chen, J. Power Sources 205 (2012) 385–393.
[8] J. Song, D.W. Shin, Y.H. Lu, C.D. Amos, A. Manthiram, J.B. Goodenough, Chem. Mater. 24 (2012) 3101–3109.
[9] M. Aklalouch, J.M. Amarill, I. Saadoune, J.M. Rojo, J. Power Sources 196 (2011) 10222–10227.
[10] H.L. Wang, T.A. Tan, P. Yang, M.O. Lai, L. Lu, J. Phys. Chem. C 115 (2011) 6102–6110.
[11] M.W. Jang, H.G. Jung, B. Scrosati, Y.K. Yun, J. Power Sources 220 (2012) 354–359.
[12] G.B. Zhong, Y.Y. Wang, X.J. Zhao, Q.S. Wang, Y. Yu, C.H. Chen, J. Power Sources 216 (2012) 368–375.
[13] L. Wang, H. Li, X. Huang, E. Baudrin, Solid State Ionics 193 (2011) 32–35.
[14] J.H. Kim, S.T. Myung, C.S. Yoon, S.G. Kang, Y.K. Sun, Chem. Mater. 16 (2012) 906–914.
[15] N. Amdouni, K. Zaghib, F. Gendron, A. Mauger, C.M. Julien, Ionics 12 (2006) 117–126.
[16] K. Dokko, M. Mohamedi, N. Anzue, T. Itoh, I. Uchida, J. Mater. Chem. 12 (2002) 3688–3693.
[17] Y. Talyosef, B. Markovsky, G. Salitra, D. Aurbach, H.J. Kimb, S. Choi, J. Power Sources 146 (2005) 664–669.
[18] Y.J. Wei, K.B. Kim, G. Chen, Electrochim. Acta 51 (2006) 3365–3373.